

Sterile Neutrino Search at the Short-Baseline Neutrino Program via Neutral Current Disappearance

A. Furmanski* and C. Hilgenberg†

School of Physics and Astronomy, University of Minnesota, Minneapolis, MN 55455, USA

(Dated: June 23, 2022)

The Short-Baseline Neutrino Program (SBN) at Fermilab, consisting of three hundred-ton-scale liquid argon time projection chambers (LAr TPCs), is well positioned to resolve a class of short-baseline neutrino oscillation anomalies that may be due to the existence of one or more sterile neutrinos. The globally allowed region for the minimal Standard Model extension with one eV-scale sterile neutrino will be largely covered at 5σ significance utilizing both ν_μ disappearance and $\nu_\mu \rightarrow \nu_e$ appearance channels. Previous sensitivities were determined utilizing charged current interactions. By taking advantage of the excellent spatial and calorimetric resolution as well as the low tracking thresholds provided by LAr TPCs, we present a novel method of estimating the neutrino energy in neutral current interactions. This method allows for the potential observation of spectral distortions in the neutral current spectrum. We use this method to perform an analysis of the statistics-only sensitivity to sterile neutrinos in the neutral current channel at SBN under a 3+1 model.

I. INTRODUCTION

Over the last few decades, a series of anomalous neutrino flavor oscillation measurements have been made at short baselines that could be explained by the existence of one or more eV-mass scale neutrinos that do not interact via any Standard Model force, so-called sterile neutrinos. To date, no long-baseline oscillation experiments have found evidence for sterile neutrinos. Global analyses have shown tension at the level of 4σ between short-baseline ν_e appearance measurements and ν_e/ν_μ disappearance measurements [1].

In the case of one eV-mass scale, stable sterile neutrino added to the Standard Model - known as a 3+1 model - at short baselines, before standard neutrino oscillations become significant, the disappearance and survival probabilities are described by Equation 1 and 2 respectively. The mixing is dominated by the last column of the 4x4 extended PMNS matrix elements, $U_{\alpha 4}$, where α refers to the neutrino flavors, $\alpha \in \{e, \mu, \tau, s\}$. Here, s refers to the new sterile flavor. The effective mixing angles are related to the 4x4 PMNS matrix elements as shown in Equations 3 and 4. Δm_{41}^2 is the mass-squared difference associated with the new sterile mass state. L and E_ν are the propagation distance and energy of the neutrino respectively.

$$P_{\nu_\alpha \rightarrow \nu_\alpha} \simeq 1 - \sin^2(2\theta_{\alpha\alpha}) \sin^2 \left(1.27 \Delta m_{41}^2 \frac{L}{E_\nu} \right) \quad (1)$$

$$P_{\nu_\alpha \rightarrow \nu_\beta} \simeq \sin^2(2\theta_{\alpha\beta}) \sin^2 \left(1.27 \Delta m_{41}^2 \frac{L}{E_\nu} \right), \quad \alpha \neq \beta \quad (2)$$

$$\sin^2(2\theta_{\alpha\alpha}) \equiv 4|U_{\alpha 4}|^2(1 - |U_{\alpha 4}|^2) \quad (3)$$

$$\sin^2(2\theta_{\alpha\beta}) \equiv 4|U_{\alpha 4}U_{\beta 4}|^2, \quad \alpha \neq \beta \quad (4)$$

Motivated by the need for a definitive resolution to the short-baseline anomalies, the Short-Baseline Neutrino Program (SBN), hosted at Fermilab, was proposed in 2015 [2]. SBN consists of three, hundred-ton scale liquid argon time projection chambers (LAr TPCs) located along the Booster Neutrino Beam (BNB) axis at distances of hundreds of meters from the BNB target. Table I summarizes the detector masses and positions. The detector positions are optimized for sterile neutrino induced oscillations with a mass-squared difference of order 1 eV². SBN sensitivity studies have focused on $\nu_\mu(\bar{\nu}_\mu)$ disappearance and $\nu_e(\bar{\nu}_e)$ appearance, identified via charged current (CC) interactions. The most recent sensitivity study [3] shows that SBN is positioned to cover the LSND 90% C.L. allowed region and most of the globally allowed regions with 5σ significance.

TABLE I: SBN detectors.

| Detector | Active Mass [tons] | BNB Target Distance [m] |
|------------|--------------------|-------------------------|
| SBND | 112 | 110 |
| MicroBooNE | 89 | 470 |
| ICARUS | 476 | 600 |

A study evaluating SBN's sensitivities over a larger range of models than the minimal 3+1 model, including 3+2 and 3+3 with a consideration of CP-violating phases, can be found in [4]. There, as in the SBN proposal, only CC interactions were considered.

In this work, we explore the possibility of applying the precision tracking, calorimetry, and low tracking threshold capabilities of LAr TPCs to the reconstruction of neutral current (NC) neutrino interactions. We present a proof of principle that the energy of the incoming neutrino can be reconstructed with sufficient resolution to enable setting unique limits within the sterile neutrino phase space, extending the physics potential of SBN. We

* afurmans@umn.edu

† chilgenb@umn.edu.

present a statistics only sensitivity analysis in the context of a 3+1 model. This is a commonly used benchmark in sterile neutrino search sensitivities. Note that sensitivities in the 3+1 case roughly translate into sensitivities in a 3+N scenario.

The flavor content of the BNB flux is about 93.6% ν_μ and 5.9% $\bar{\nu}_\mu$ with contamination from ν_e and $\bar{\nu}_e$ at the level of 0.5% below energies of 1.5 GeV. Given the low level of contamination from ν_e 's and $\bar{\nu}_e$'s, their contribution to the NC disappearance signal will be neglected in our analysis.

In a sterile neutrino search based on NC interactions, the signal is the disappearance of any active neutrinos. NC disappearance, quantified by $1 - P_{\nu_\mu \rightarrow \nu_s}$, provides the only means of directly constraining $|U_{s4}|$. Note that the disappearance probability is the same for $\bar{\nu}_\mu$'s. The corresponding effective mixing angle, $\sin^2(2\theta_{\mu s})$, can be related to other mixing angles being probed at SBN by imposing unitarity on the 4x4 PMNS matrix (Eq. 5), yielding the relation shown in Eq. 6, providing a link between the $\nu_\mu/\bar{\nu}_\mu$ disappearance, $\nu_\mu \rightarrow \nu_e/\bar{\nu}_\mu \rightarrow \bar{\nu}_e$ appearance, and $\nu_\mu \rightarrow \nu_\tau/\bar{\nu}_\mu \rightarrow \bar{\nu}_\tau$ appearance mixing angles.

$$1 = \sum_{i=e,\mu,\tau,s} |U_{i4}|^2 \quad (5)$$

$$\sin^2 2\theta_{\mu s} = \sin^2 2\theta_{\mu\mu} - \sin^2 2\theta_{\mu e} - \sin^2 2\theta_{\mu\tau} \quad (6)$$

A. Constraints on PMNS Matrix Elements

Eq. 6 demonstrates the additional physics reach that could be provided to SBN by the addition of a NC disappearance search. In addition to providing complementary information to the SBN ν_μ disappearance and ν_e appearance analyses, a NC disappearance search at SBN can provide unique constraints on the 3+1 phase space.

Past sterile neutrino searches have contributed to a growing collection of data sets, providing constraints on $|U_{e4}|$ and $|U_{\mu 4}|$. There are relatively few constraints on $|U_{\tau 4}|$ due to the lack of a ν_τ source and the few-GeV energy threshold for ν_τ CC interactions, nearly beyond the reach of most neutrino sources. To date, the most stringent constraint on $|U_{\tau 4}|$ comes from atmospheric neutrinos, IceCube [5] in particular. The IceCube measurements utilize the MSW effect to probe $|U_{\tau 4}|$ via CC interactions.

We are aware of only a single experiment that has set limits in the case of a sterile neutrino NC disappearance search, NO ν A [6]. Both IceCube and NO ν A set mutually consistent limits in the $(|U_{\mu 4}|, |U_{\tau 4}|)$ plane with the IceCube limit being more stringent. Nevertheless, the NC probe is more direct, relying on fewer model assumptions.

Since NO ν A operates at a long baseline, their active flavor oscillation signal competes with any sterile neutrino signal. This is not the case at short baselines.

With a NC analysis, SBN would provide the first short-baseline, and therefore most direct, constraint on $|U_{\tau 4}|$ to date.

In evaluating the impact of a NC analysis at SBN, it is useful to compare our sensitivities to the globally allowed phase space. However, this is difficult in that, to our knowledge, a global analysis of sterile neutrino induced NC disappearance does not exist. In order to provide some baseline with which we can benchmark our performance, we used the globally allowed values of the PMNS matrix elements, specified for two values of Δm_{41}^2 , found in [5]. This supplies four points in the $(\sin^2 2\theta_{\mu s}, \Delta m_{41}^2)$ plane after applying Equations 3, 4, and 6. While the allowed region that this procedure produces is likely not complete, it does provide a reasonable set of values to which we can compare limits that we produce. Global analyses of sterile neutrino searches and likewise calculating globally allowed regions in phase space is difficult. For more discussion, [7] gives a summary of the current status and challenges of sterile neutrino searches.

In the following sections, we introduce two different methods for reconstructing the neutrino energy in NC interactions: a conventional method based on visible energy in the detector and a novel method that applies the unique capabilities of LAr TPCs. Both are sensitive to the presence of certain sterile neutrinos, and we show that a combination of the two methods performs better than either method alone.

II. NEUTRINO ENERGY RECONSTRUCTION IN NEUTRAL CURRENT INTERACTIONS

In NC interactions, the scattering neutrino carries away some fraction of its initial energy as illustrated in Fig. 1. A trivial upper bound on the neutrino energy can be obtained by summing over all visible deposited energy associated with a neutrino vertex candidate. This calorimetric method leads to significant underestimation of the neutrino energy, as large as 90% (Fig. 2). Nevertheless, the calorimetric method has been used with success in some experiments, NO ν A [6] for example.

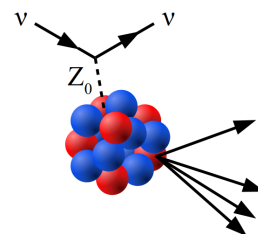


FIG. 1: A neutrino scatters off a nucleon, carrying away some fraction of its initial energy, producing a final state hadronic system that can be used to determine the incident neutrino energy.

A. A New Method

Compared to water Cherenkov and scintillator based detectors, LAr TPCs provide low tracking thresholds and precise energy and angular resolution for charged particles. These capabilities motivate a new reconstruction model based on the kinematics of the final state hadronic system. We have developed a kinematic method that, using some simplifying assumptions, uniquely determines the initial neutrino energy, accounting for the energy carried away by the neutrino. We assume that the neutrino scatters off a single nucleon at rest. If we ignore nuclear effects, including nucleon-nucleon correlation, nuclear recoil, and binding energy, the incoming neutrino energy can be determined from the energy and momentum of the final state hadronic system.

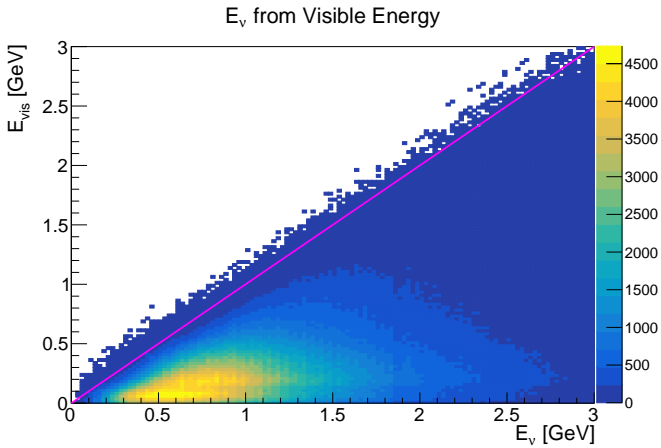


FIG. 2: The visible hadronic energy (y-axis) in neutral current interactions plotted against the true neutrino energy (x-axis) shows that calorimetry alone provides a poor estimate of the neutrino energy.

In the lab frame, the initial state neutrino and nucleon four momenta are given by $p_{\nu,i}^\mu = (E_\nu, 0, 0, p_\nu)$ and $p_{N,i}^\mu = (m_N, 0, 0, 0)$. The z-axis is aligned with the neutrino beam direction. In the final state, also in the lab frame, the outgoing neutrino is unmeasured, but the four momentum of the hadronic system can be described by $p_h^\mu = (E_h, \mathbf{p}_h)$. From this, we calculate the initial neutrino energy in terms of the final state hadronic system kinematics, shown in Equation 7 where θ_h is the hadronic system angle with respect to the beam direction ($\cos \theta_h = \mathbf{p}_h \cdot \hat{z} / |\mathbf{p}_h|$). The hadronic four-momentum is calculated by summing the four-momenta of all visible particles. This method is analogous to the CC energy reconstruction used by T2K and MiniBooNE, based on the quasi-elastic assumption when only the final state lepton is observed.

$$E_\nu^{\text{reco}} = \frac{p_h^2 - (E_h - m_N)^2}{2(m_N + p_h \cos \theta_h - E_h)} \quad (7)$$

Figure 3, with the reconstructed neutrino energy plotted as a function of the true neutrino energy, demonstrates the validity of our method. The figure was obtained from a NC inclusive selection. Compared to the calorimetric method, the distribution obtained with our method is peaked along the diagonal.

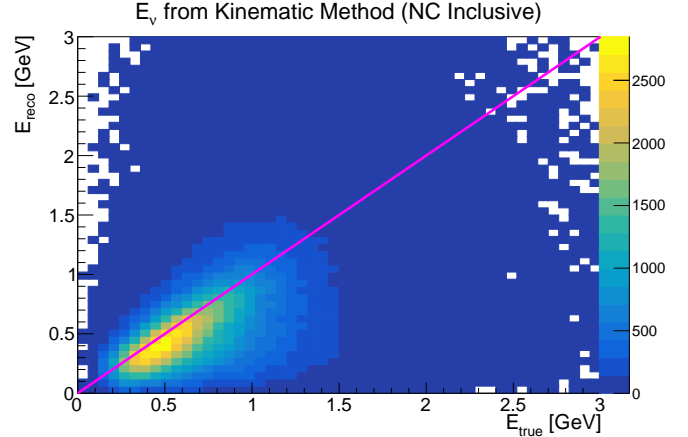


FIG. 3: The reconstructed neutrino energy using our model (x-axis) plotted against the true neutrino energy (y-axis) for neutral current inclusive events shows reasonable agreement. There is clearly a strong correlation between the two variables. This is to be compared to Fig 2 where only calorimetry is used.

With the potential gains of our new method established, we now describe how we apply detector effects in our analysis.

B. Adding Detector Effects

We evaluate the performance of our kinematic method using a sample of five million ν_μ and $\bar{\nu}_\mu$ interactions on argon, each generated using GENIE v3.0.0 with the default tune. The BNB flux prediction at each SBN detector is used to generate detector specific samples. A combination of the flux and detector active mass is used to generate a factor for scaling each flux component in terms of protons on target (POT).

For simplicity, we forgo a full detector simulation and assume Gaussian angular and energy resolutions for the final state particles. Table II summarizes a reasonable range of resolutions by particle type. In addition, the tracking thresholds, applied to the true kinetic energy, are provided. The ranges of possible reconstruction performances are taken from published MicroBooNE analyses [8][9][10][11].

If particle species not listed in Table II are present in a given NC event, with the exception of neutrons or neutral pions, the event is excluded from the analysis. This results in a negligible loss in sample size while making the interpretation of our results more straightforward.

TABLE II: Assumed performances for LAr TPCs are given for species of interest. Charged pions with momenta below 300 MeV/c are assumed to have similar reconstruction performances as muons. The threshold is set by the requirement that two or more TPC wires are crossed and is applied to the true kinetic energy.

| Species | Thresh. [MeV] | Energy Res. | Angular Res. [deg] |
|---------------------|---------------|-------------|--------------------|
| p [8] | 25-50 | 60 MeV | 5-10 |
| $\pi^{+/-}$ [9][10] | 10-20 | 10-20% | 2-5 |
| γ [11] | 30 | 10-20% | 5-10 |

In comparing reconstruction performances between the calorimetric and kinematic methods, discussed next, we adopt the most optimistic choice of the performances listed in Table II.

C. Evaluating Reconstruction Performance

In order to evaluate the reconstruction performance of each reconstruction method, we first compare the neutrino energy resolutions. Next, we compare the reconstruction efficiencies. In both cases, we consider different sample selections. We adopt a NC inclusive selection for the calorimetric method. For the kinematic method, we investigated several exclusive final state topologies. Here, we show results for NC inclusive as well as single proton final states (NC1p).

The most significant driver for underestimating the incident neutrino energy in CC or NC interactions is neutrons. LAr TPCs have some ability to observe neutrons either through deexcitation photons produced in neutron capture or through the production of charged hadrons in inelastic scatters. We neglect deexcitation photons and conservatively estimate that we can tag neutrons (n-tagging) via inelastic scatters with kinetic energies above 50 MeV with 50% efficiency. If one or more neutrons are tagged, we make no attempt to estimate the energy of the scattering neutron(s) and reject the whole event. This cut has been applied for the kinematic method with NC1p selection only.

The absolute energy resolution is plotted in Fig. 4 while the fractional resolution is plotted in Fig. 5. Results are shown for calorimetric NC inclusive, kinematic NC inclusive, and kinematic NC1p with n-tagging methods and selections. From both figures, it is evident that kinematic method provides a less biased estimate of the neutrino energy.

The model assumptions underlying our kinematic method are valid primarily for quasi-elastic neutrino scattering, the dominant process at BNB energies, as evidenced by the best neutrino energy resolution being obtained with the NC1p with n-tagging selection. However, other processes are significant such as meson exchange current, resonant production, and deep inelastic scattering.

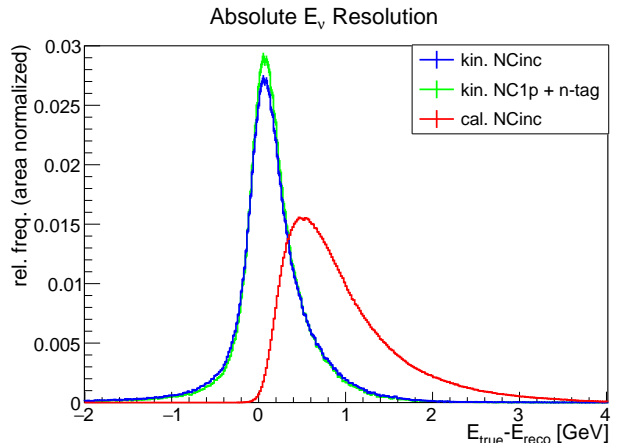


FIG. 4: Absolute energy resolution obtained with different reconstruction methods shows that the kinematic method has better energy resolution and lower bias than the calorimetric method. Each distribution has been area normalized.

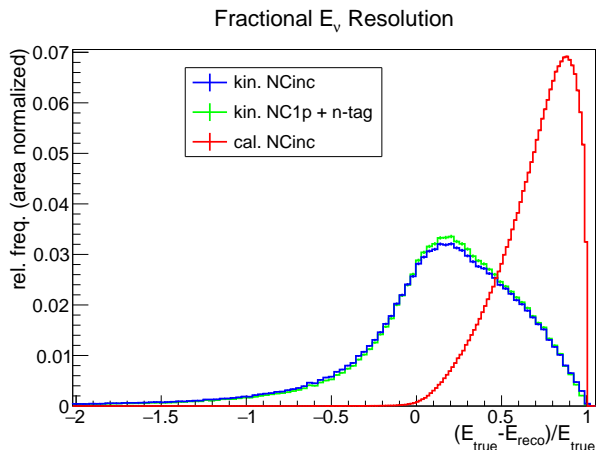


FIG. 5: Fractional energy resolution obtained with different reconstruction methods shows that the kinematic method has better energy resolution than the calorimetric method. Each distribution has been area normalized.

There is a long tail in the neutrino energy fractional resolution distribution where the energy is overestimated. This is primarily driven by the failure of our model assumptions, the nucleon-nucleon correlations and the nucleon Fermi momentum in particular. In some cases, invalid model assumptions result in a negative reconstructed neutrino energy; these events are rejected.

Table III summarizes the energy resolution and bias associated with each reconstruction method and sample selection discussed above. These results quantitatively demonstrate that the kinematic method provides 73-78% lower bias and 31-44% lower full width at half maximum (FWHM) compared to the calorimetric method.

The primary limitation on the utility of our method

TABLE III: The neutrino energy bias and resolution is summarized for the two different reconstruction methods with different sample selections.

| Method and Selection | Bias [MeV] | FWHM [MeV] |
|------------------------------|------------|------------|
| Calorimetric NCinc | 665 | 792 |
| Calorimetric NC0 $\pi^{+/-}$ | 662 | 792 |
| Kinematic NCinc | 172 | 545 |
| Kinematic NC0 $\pi^{+/-}$ | 178 | 495 |
| Kinematic NC1p + n-tag | 140 | 446 |

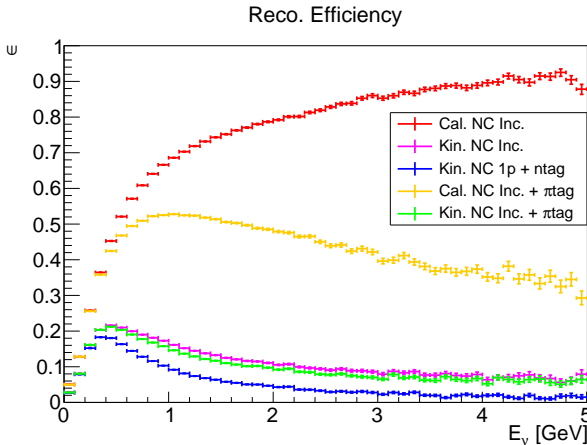


FIG. 6: The reconstruction efficiency (y-axis) is plotted as a function of the true neutrino energy (x-axis) for the two different reconstruction methods, calorimetric or kinematic, and different sample selections.

is the efficiency. While the kinematic method provides superior neutrino energy resolution compared to the conventional calorimetric method, it incurs inefficiencies when the assumptions of the model fail. This is demonstrated in Figure 6. It should be noted, however, that LAr TPC detectors at these energies struggle to differentiate between muons and pions, each having nearly identical energy loss as a function of range. It is not unreasonable to assume, therefore, that to eliminate ν_μ CC background contributions, events with charged pions in the final state may need to be rejected. Adding a requirement that there are no final state charged pions, the efficiency of the calorimetric method is more significantly affected than that for our method as demonstrated by the integrated efficiencies for the different reconstruction

TABLE IV: Integrated efficiencies are provided for the different reconstruction methods and event selections.

| Method and Selection | Integrated Efficiency |
|------------------------------|-----------------------|
| Calorimetric NCinc | 0.60 |
| Calorimetric NC0 $\pi^{+/-}$ | 0.47 |
| Kinematic NCinc | 0.17 |
| Kinematic NC0 $\pi^{+/-}$ | 0.16 |
| Kinematic NC1p + n-tag | 0.13 |

methods and event selections, shown in Table IV. Nevertheless, even with a charged pion veto the calorimetric method dominates in terms of statistical power.

Having demonstrated the benefits and limitations of our new reconstruction method, we now consider the role a NC analysis would play in the sterile neutrino search at SBN.

III. APPLYING NEUTRAL CURRENT RECONSTRUCTION AT SBN

We have established that the conventional calorimetric method is better in terms of efficiency while our new kinematic method performs better in reconstructing the neutrino energy. In this section, we apply each reconstruction method to the search for sterile neutrinos at SBN via a NC disappearance search.

We demonstrate that the calorimetric and kinematic methods are each sufficient for observing spectral features that are characteristic of neutrino disappearance. This is important not only for observing disappearance but also for determining the values of the mixing parameters, Δm_{41}^2 and $\sin^2 2\theta_{\mu s}$. We present a comparison of the true and reconstructed neutrino energy spectra at each SBN detector. Next, we quantify our sensitivity to eV-scale sterile neutrinos in the context of the minimal 3+1 model. We show exclusion limits followed by allowed regions for selected nonzero mixing parameters.

For this analysis, each of the detector specific samples is scaled to the expected exposure provided in the SBN proposal: 6.6×10^{20} POT for SBND and ICARUS, 13.2×10^{20} POT for MicroBooNE. Backgrounds from ν_μ CC events are neglected as we consider only exclusive NC0 $\pi^{+/-}$ samples, identified by the reconstruction, for the sensitivity analysis. We do anticipate some background from beam induced activity in materials surrounding the argon active volume, so-called dirt events. These are not expected to comprise a significant fraction of our NC events. However, dirt backgrounds will be addressed in followup studies using a full detector simulation and reconstruction.

As in the previous section, we present sensitivities for the calorimetric method with NC0 $\pi^{+/-}$ selection, the kinematic method with NC0 $\pi^{+/-}$ selection, and the kinematic method with NC1p and n-tagging selection.

A. Neutrino Energy Spectra

To illustrate the power of resolving spectral features in observing oscillation effects, Figures 7 and 8 show NC neutrino energy spectra at each SBN detector. The null hypothesis, absence of short-baseline oscillations, is compared to a case with $\sin^2 2\theta_{\mu s} = 0.0403$ and $\Delta m_{41}^2 = 1 \text{ eV}^2$ (Fig. 7) or $\Delta m_{41}^2 = 7 \text{ eV}^2$ (Fig. 8). These values are taken from the edge of the globally allowed region in the 3+1 phase space obtained following the procedure

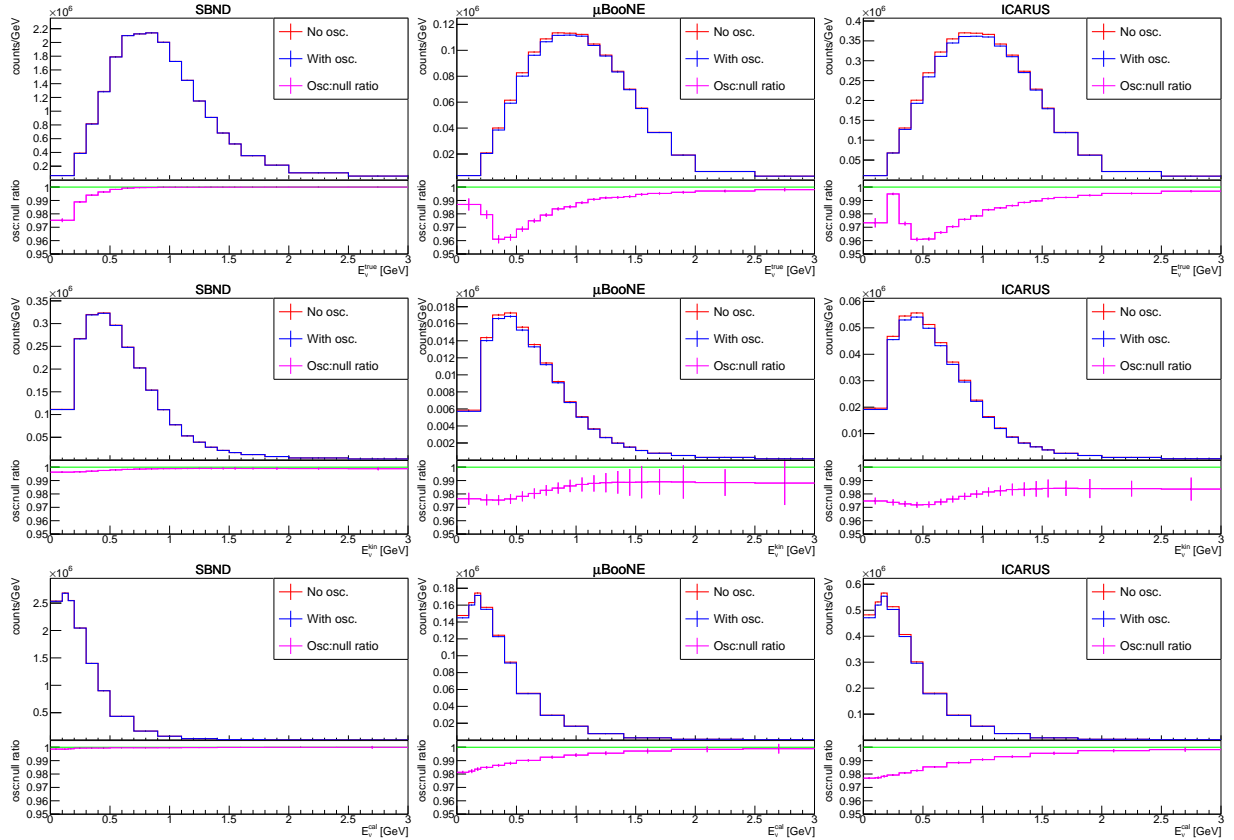


FIG. 7: A comparison between reconstructed neutral current neutrino energy spectra cases with no oscillation and with $\Delta m_{41}^2 = 1 \text{ eV}^2$, $\sin^2 2\theta_{\mu s} = 0.04$ is shown for each SBN detector: SBND (left column), MicroBooNE (center column), and ICARUS (right column). The true (top row) spectra are shown as well as the reconstructed spectra using the kinematic method with NC1p and neutron tagging selection (center row) and the calorimetric method with NC inclusive selection (bottom row).

described in the introduction. The L/E_ν behavior of the oscillations is evident. A clear, energy dependent depletion in events is observable in the near detector for both values of Δm_{41}^2 while the energy dependent depletion at MicroBooNE and ICARUS is primarily only resolvable at lower values.

Comparing the calorimetric and kinematic methods, we see that the kinematic method performs better in pinpointing the location of the oscillation maximum. While the calorimetric method yields some shape information, it does not directly provide the oscillation peak location, however it has the sizeable advantage of significantly higher statistics. Comparing the low- and high- Δm_{41}^2 cases shows how both methods have sensitivity to the true energy spectral distortions. In the following subsection we describe how the advantages of both methods may be combined to boost the oscillation sensitivity.

B. Oscillation Sensitivity

In order to evaluate the sensitivity of our method within the scope of SBN, we adopt a binned Poisson like-

likelihood approach to evaluate the statistical significance of a 3+1 signal compared to the null hypothesis. We construct a log likelihood ratio (LLR) as shown in Eq. 8 and assume Wilk's Theorem applies so that the significance is $\sigma = \sqrt{\Delta\chi^2} = \sqrt{\mathcal{L}}$. We use an approximate form of the LLR obtained through application of Sterling's approximation for LLR calculations, shown in Eq. 9. The index runs over bins of reconstructed neutrino energy across all three SBN detectors. For consistency, we verified that our analysis methods produce a similar result for the 3+1 statistics-only ν_μ disappearance sensitivity analysis as in [4].

$$\mathcal{L} = -2 \prod_i^N \left[\frac{(N_i^{obs})^{N_i^{null}}}{N_i^{null}!} e^{-N_i^{obs}} \right] \quad (8)$$

$$\mathcal{L} \approx 2 \sum_i^N \left[N_i^{obs} - N_i^{null} + N_i^{null} \ln \frac{N_i^{null}}{N_i^{obs}} \right] \quad (9)$$

Our neutral current disappearance sensitivity for the kinematic method using a NC1p with neutron tagging

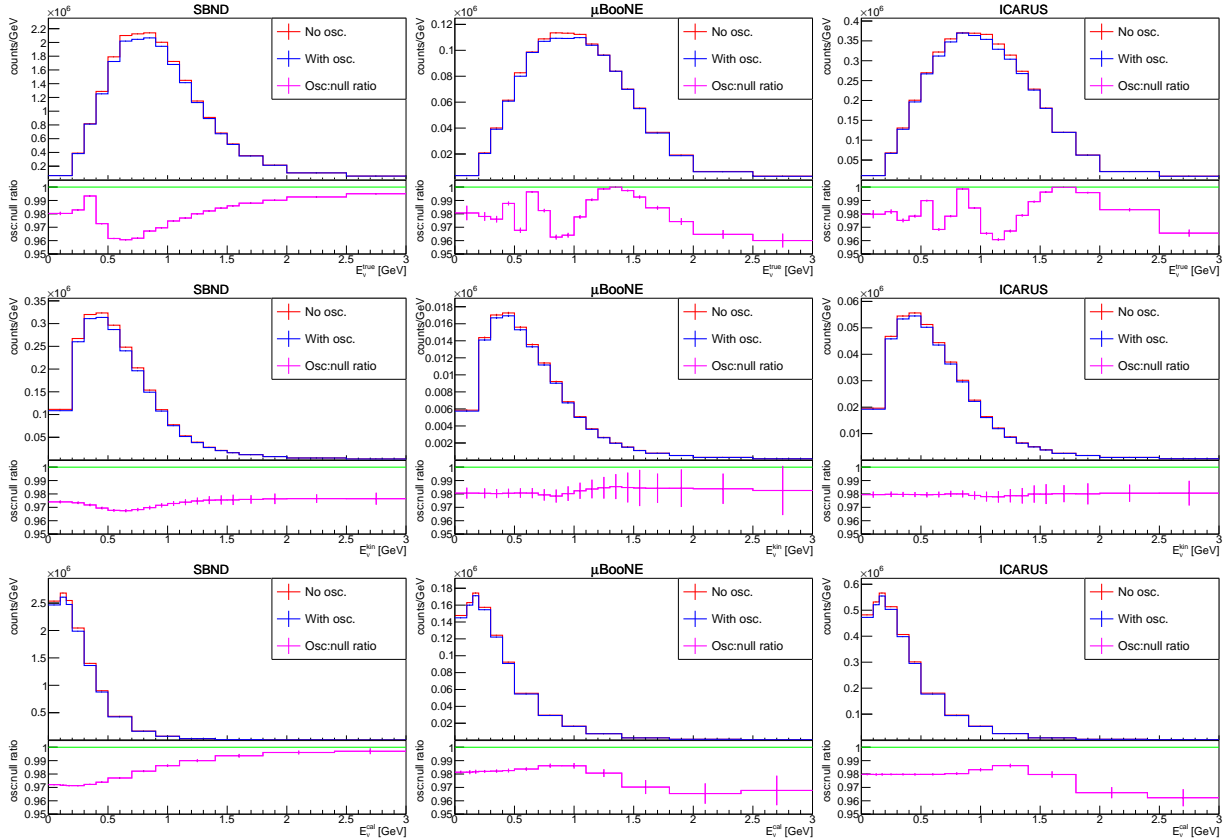


FIG. 8: A comparison between reconstructed neutral current neutrino energy spectra cases with no oscillation and with $\Delta m_{41}^2 = 7 \text{ eV}^2$, $\sin^2 2\theta_{\mu s} = 0.04$ is shown for each SBN detector: SBND (left column), MicroBooNE (center column), and ICARUS (right column). The true (top row) spectra are shown as well as the reconstructed spectra using the kinematic method with NC1p and neutron tagging selection (center row) and the calorimetric method with NC inclusive selection (bottom row).

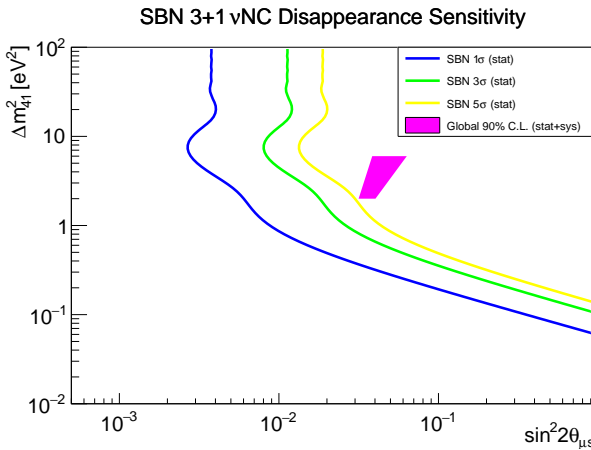


FIG. 9: Using the kinematic reconstruction method with NC1p and neutron tagging selection, exclusion contours are shown for a three detector fit at SBN including statistical uncertainties only. 1 σ , 3 σ , and 5 σ contours are shown along with the globally allowed 90% C.L. that includes both statistical and systematic uncertainties [5].

selection is shown in Fig. 9 with 1 σ , 3 σ , and 5 σ contours drawn in $(\sin^2 2\theta_{\mu s}, \Delta m_{41}^2)$ space. These contours include statistical uncertainties only. The addition of systematic uncertainties is expected to reduce sensitivity primarily for $\Delta m_{41}^2 > 1 \text{ eV}^2$ where the oscillation probability begins to vary rapidly with neutrino energy. For comparison, globally allowed values from [5], which include statistical and systematic uncertainties, are shown to be covered with 5 σ significance.

While our kinematic reconstruction method is sufficient to cover the globally allowed region with 5 σ significance, its limited efficiency yields a weaker NC disappearance sensitivity compared to the conventional (calorimetric) method. This motivates a multi-sample approach where we combine the kinematic and calorimetric methods - we want to extract the more accurate shape information with the kinematic method while maintaining the same reconstruction efficiency as the calorimetric method.

In applying the kinematic method, we choose two different sample selections: NC1p with neutron tagging and NC inclusive. The NC1p sample provides better neutrino energy resolution than the NC inclusive selection

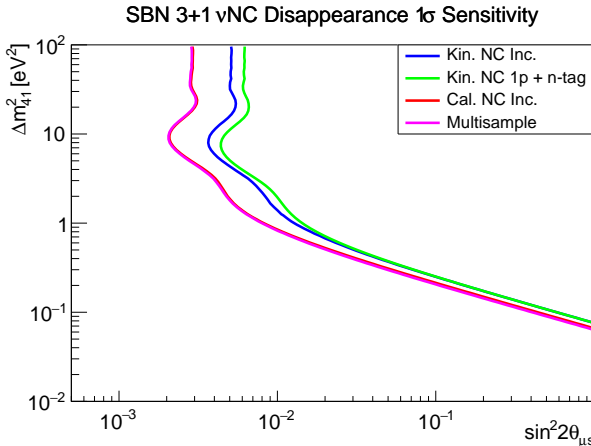


FIG. 10: 1σ exclusion contours are shown for a three detector fit at SBN including statistical uncertainties only for the different reconstruction methods and sample selections.

while both provide better resolution than the calorimetric method. This motivates a three step reconstruction sequence where we generate three statistically independent samples. First, the kinematic method with NC1p and neutron tagging selection is applied. Any events rejected are passed to the kinematic method with NC inclusive selection. Finally, any events rejected in this step are passed to the calorimetric NC inclusive reconstruction.

1σ exclusion limits for the four different methods and selections are shown in Fig. 10. The statistical power of the calorimetric method is evident compared to kinematic method selections. In the multi-sample selection that maintains the same overall sample size as the calorimetric method, the added shape information from the kinematic reconstruction leads to a marginal, percent-level improvement in sensitivity.

Note that it is possible to improve the limits shown in Fig. 10 in some regions of phase space by increasing the sample size at the far detector. For larger values of Δm_{41}^2 , the limits are expected to be systematics limited, driven by the shape measurement in the near detector. For smaller Δm_{41}^2 , however, the limits are limited by the far detector statistics. For example, a doubling of the planned exposure at the far detector results in an approximate 50% sensitivity improvement for $\Delta m_{41}^2 < 4 \text{ eV}^2$.

The power of the multi-sample approach becomes more evident when considering the ability to pinpoint the oscillation parameters in the presence of a disappearance signal where shape information is crucial. Figures 11 and 12 show the 1σ allowed regions for the same mixing parameter values shown in Figures 7 and 8. In both cases, the multi-sample fit clearly outperforms the calorimetric method alone. This is especially true at lower values of Δm_{41}^2 before the oscillations become too rapid to resolve at the intermediate and far detectors.

Additionally, we expect the use of two different energy estimation methods will provide a way of cross-checking

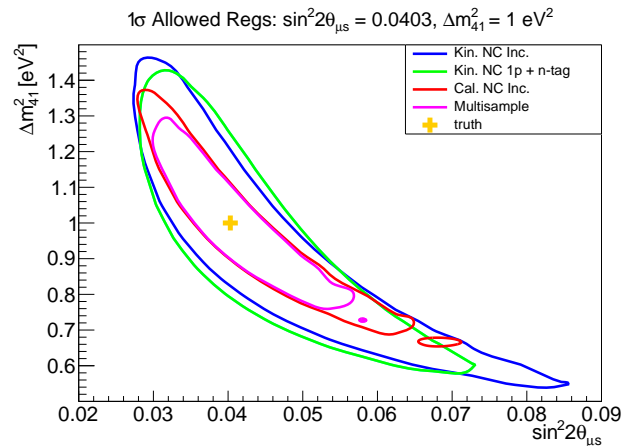


FIG. 11: For the case with $\Delta m_{41}^2 = 1 \text{ eV}^2$ and $\sin^2 2\theta_{\mu s} = 0.04$, 1σ allowed regions are shown for a three detector fit at SBN including statistical uncertainties only for the different reconstruction methods and sample selections.

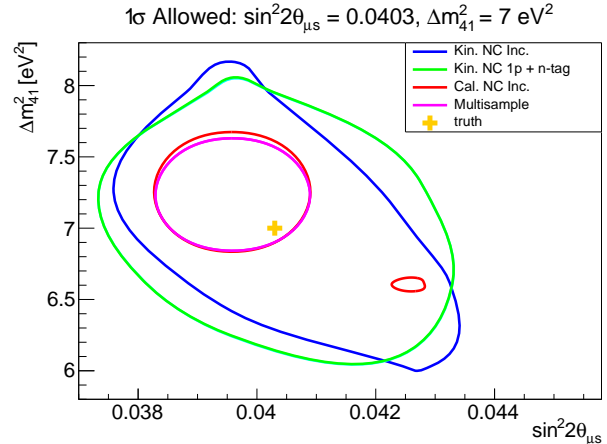


FIG. 12: For the case with $\Delta m_{41}^2 = 7 \text{ eV}^2$ and $\sin^2 2\theta_{\mu s} = 0.04$, 1σ allowed regions are shown for a three detector fit at SBN including statistical uncertainties only for the different reconstruction methods and sample selections.

biases from interaction modelling uncertainties, reducing the final systematic uncertainty.

IV. CONCLUSIONS AND OUTLOOK

The excellent calorimetry and tracking capabilities and low tracking thresholds of liquid argon time projection chambers provide an opportunity to apply neutral current interactions to the sterile neutrino search at the Short-Baseline Neutrino Program (SBN). We have introduced a new energy estimation method for neutral current interactions based on the kinematics of the final state hadronic system. We demonstrated that our method can

provide sufficient energy resolution and efficiency to cover globally allowed regions of the 3+1 sterile neutrino phase space with 5σ significance, though systematic uncertainties will reduce this.

While our method provides superior energy resolution compared to the conventional calorimetric method, it suffers from low efficiency. In combining our method with the conventional one in a multi-sample approach, we showed that we can push oscillation sensitivities beyond what is possible with the conventional method alone.

The addition of a neutral current disappearance search to the SBN physics program can significantly enhance the physics reach of SBN, providing both complimentary and redundant information that can serve to overconstrain the sterile neutrino phase space in the currently considered ν_μ disappearance and ν_e appearance channels in addition to providing unique limits on the poorly constrained 3+1 PMNS matrix element $U_{\tau 4}$.

With the proof of concept provided in this work, we will implement our reconstruction approach in the SBN simulation and reconstruction framework. We will test our method using a full simulation and reconstruction and reevaluate the performances presented in this work.

Finally, the neutral current analysis will be integrated into the oscillation sensitivity analysis framework to provide the most realistic sensitivity projections.

While we wait for SBN to accumulate data, we can take advantage of the data set obtained by MicroBooNE to test our reconstruction method. This is a crucial step as the performance we have presented here is model dependent. For example, if nuclear effects are more or less significant, this will have an impact on the energy resolution and selection efficiency of the neutral current analysis and therefore the sensitivities presented in this work. To this end, we can make use of charged current interactions, replacing the outgoing neutrino in our model with the outgoing lepton. This will provide a reliable test of using the kinematics of the final state hadronic system as an estimator of the incoming neutrino energy.

ACKNOWLEDGMENTS

This work was supported by funding from the University of Minnesota.

[1] M. Dentler, Á. Hernández-Cabezudo, J. Kopp, P. A. N. Machado, M. Maltoni, I. Martinez-Soler, and T. Schwetz, Updated global analysis of neutrino oscillations in the presence of ev-scale sterile neutrinos, *Journal of High Energy Physics* **2018**, 1 (2018).

[2] R. Acciarri, *et al.* (MicroBooNE, LAr1-ND, and ICARUS-WA104 collaborations), A proposal for a three detector short-baseline neutrino oscillation program in the fermilab booster neutrino beam (2015), arXiv:1503.01520 [physics.ins-det].

[3] P. A. Machado, O. Palamara, and D. W. Schmitz, The short-baseline neutrino program at fermilab, *Annual Review of Nuclear and Particle Science* **69**, 363 (2019), <https://doi.org/10.1146/annurev-nucl-101917-020949>.

[4] D. Cianci, A. Furmanski, G. Karagiorgi, and M. Ross-Lonergan, Prospects of light sterile neutrino oscillation and cp violation searches at the fermilab short baseline neutrino facility, *Phys. Rev. D* **96**, 055001 (2017).

[5] G. H. Collin, C. A. Argüelles, J. M. Conrad, and M. H. Shaevitz, First constraints on the complete neutrino mixing matrix with a sterile neutrino, *Phys. Rev. Lett.* **117**, 221801 (2016).

[6] S. Yang, *Searching for Light Sterile Neutrinos with NOvA Through Neutral-Current Disappearance*, Ph.D. thesis, Cincinnati U. (2019).

[7] A. Diaz, C. Argüelles, G. Collin, J. Conrad, and M. Shaevitz, Where are we with light sterile neutrinos?, *Physics Reports* **884**, 1 (2020).

[8] P. Abratenko *et al.* (MicroBooNE Collaboration), Measurement of differential cross sections for ν_μ -ar charged-current interactions with protons and no pions in the final state with the microboone detector (2020), arXiv:2010.02390 [hep-ex].

[9] P. Abratenko *et al.* (MicroBooNE Collaboration), First measurement of differential charged current quasielastic-like ν_μ -argon scattering cross sections with the microboone detector, *Phys. Rev. Lett.* **125**, 201803 (2020).

[10] P. Abratenko *et al.* (MicroBooNE Collaboration), First measurement of inclusive muon neutrino charged current differential cross sections on argon at $E_\nu \sim 0.8$ GeV with the microboone detector, *Phys. Rev. Lett.* **123**, 131801 (2019).

[11] C. Adams, M. Alrashed, R. An, J. Anthony, J. Asaadi, A. Ashkenazi, S. Balasubramanian, B. Baller, C. Barnes, G. Barr, *et al.*, Reconstruction and measurement of $\mathcal{O}(100)$ mev energy electromagnetic activity from $\pi^0 \rightarrow \gamma\gamma$ decays in the microboone lartpc, *Journal of Instrumentation* **15** (02).